ICAS 2016
30th Congress of the International Council of the Aeronautical Sciences
DCC, Daejeon, Korea ; September 25-30, 2016

COUPLED EMC-THERMAL MODELING OF ELECTRICAL HARNESSES WITHIN "MORE ELECTRICAL AIRCRAFT"

Florian MAHIDDINI*, Michael RIDEL*, Philippe REULET*, David DONJAT*, Pierre MILLAN*.
***ONERA – The French Aerospace Lab** - *florian.mahiddini@onera.fr*

Keywords: More Electrical Aircraft, Transmission Line Theory, Heat Transfer, EMC

Abstract

In this paper, an original method has been developed in order to compute simultaneously primary per unit length electrical parameters and temperature field of complex wiring. The suggested strategy, based on topological description of the electrical network and the use of integral equations, was applied to a realistic cable bundle. Numerical experiments, conducted with specifically designed tools, highlighted the significant role played by electromagnetic coupling on the heating of a group of cables.

1) Context

In recent years, the part of electricity used as auxiliary power source (i.e. for non propulsive purpose) has kept growing and will continue to increase, given that electricity has considerable advantages compared to hydraulic or pneumatic powers. This trend, known as "More Electrical Aircraft" (MEA), leads to an increase of the number of cables in the embedded Electrical Wiring Interconnection System (EWIS) **[1]**.

Hence, being able to model correctly Electromagnetic Compatibility (EMC) and thermal constraints on those cables thereby becomes more and more stringent for future MEA developments **[2]**. However, nowadays these constraints are studied separately (see Fig. 1), which means that physical interactions between both EMC and thermal models are not taken into account and finally leads to a non optimal mass of the whole cable system.

Therefore, the aim of this paper is twofold. Firstly, we will describe the mainlines of the two EMC and thermal models developed at ONERA. Secondly, we will detail a common methodology for managing both constraints within the same computation procedure to allow, for future developments, optimization on the embedded mass and design of the EWIS.

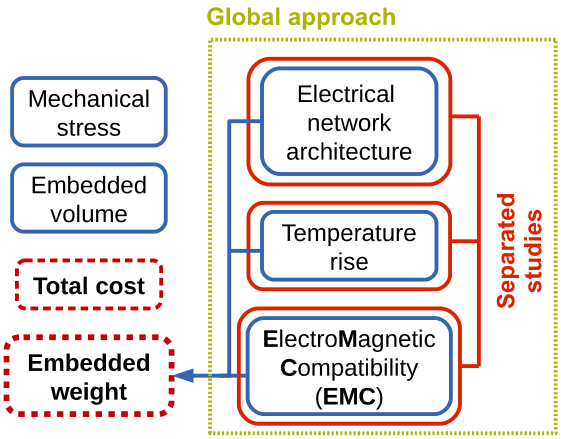

Fig. 1: Main constraints applied on an EWIS and need for a global approach

2) Topological description of the network

To model a large EWIS as those embedded on aircraft, one has first to reduce its complexity. The topological approach is well-suited for such a purpose by enabling the representation of the whole electrical network with only few elements.

Thus, each identified group of cables sharing the same geometry or operating conditions are modeled inside the same *tube* as a uniform transmission line. This classification was first applied at ONERA for EMC applications and selection criteria were defined

according to electromagnetic considerations like, for example, the distance to a reference ground plane. Nevertheless, this topological description can not only be seen from an electromagnetic point of view but thermal as well, which constitutes the original part of our work. Consequently, parameters like ambient temperature or pressure that can impact heat transfer at harness level are also included in the definition of *tubes* and can result in slightly different topological representations as depicted in Fig. 2.

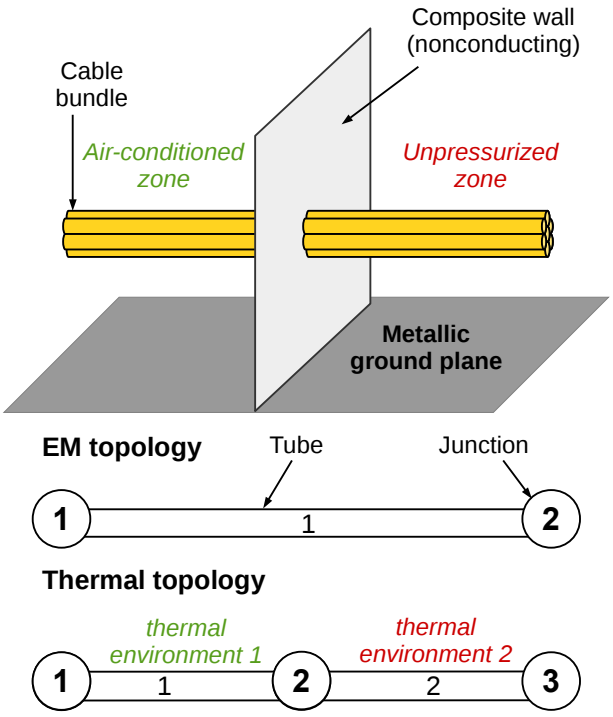

Fig. 2: Difference between EM and thermal topology representation

In this example, a cable bundle crosses two different thermal environments while from an electromagnetic approach its situation has not changed. This observation is still true in the event where electromagnetic parameters (due to a shift of bundle installation for example) change along the wiring while thermal ones do not. This fact illustrates that both EM and thermal topological views can be seen as specific refinements of a more general topological tree.

Once this topological step is established, the next phase of the description is to define for each *tube* its own physically representative cross-section that takes into account installation conditions. *Junctions* of the network interconnecting *tubes* are modeled with nodes in the topological tree. These junctions ensure electrical and thermal continuity over the tubes network. They also represent load impedance or heating equipment depending on which point of view one stands.

An example of a complete topological tree for a possible MEA architecture is given on Fig. 3.

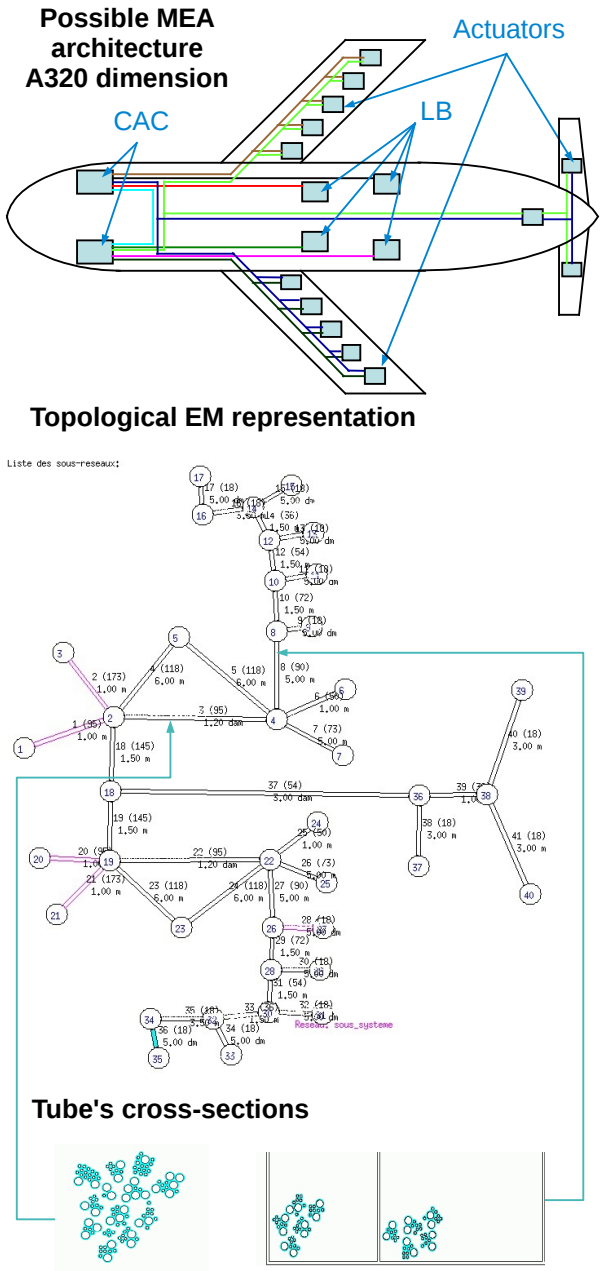

Fig. 3: General topological representation of an MEA architecture

3) EMC modeling

Multiplication of EMI sources as well as the rise of frequency in systems operations can lead to critical malfunctions between electrical devices. Wiring network represents a very special issue for electromagnetic study because cables are spread throughout the structure and can be both source and receiver of interferences. To avoid that such coupling phenomena jeopardize the safety of the aircraft, EMC study has to be conducted as soon as possible in the development cycle.

To restrict the use of heavy experimental setups, ONERA has developed for many years its own software suite called *CRIPTE™*, whose objectives are to predict and quantify propagation and coupling phenomena that are generated on the wiring network. In this framework, principles of electromagnetic topology have been coupled to the theory of "multiconductor transmission line network" (MTLN). Hence the whole system is split into several sub-systems and the resolution procedure can be divided into three major steps as further presented below **[3] [4]**.

3.1) Multiconductor Transmission Line Model

The Transmission Line theory is based under the assumption of transverse electromagnetic (TEM) modes propagating along the wiring. This approximation can be made because cross dimensions of the wiring are often negligible in front of the wavelength of carried signals, which in return limits the use of this formalism to hundreds MHz.

Consequently, within its validity domain, this TEM mode assumption greatly simplifies Maxwell's equations and yields to the following expressions of the transverse electric and magnetic field :

$$\boldsymbol{H}_T = \frac{1}{\eta} z \times \boldsymbol{E}_T$$
$$\nabla_T \times \boldsymbol{E}_T = 0 \text{ and } \nabla_T . \boldsymbol{E}_T = 0 \qquad (1)$$

where η represents the characteristic impedance of the dielectric medium between conductors. We can notice that the two expressions linked to $\boldsymbol{E}_T$ can be expressed as a single gradient of the scalar electrostatic potential $\boldsymbol{\Phi}$.

Thus, the electromagnetic field can be obtained from an equivalent electrostatic problem which has the type of a Laplace's equation :

$$\nabla . (\epsilon \nabla \boldsymbol{\Phi}) = 0 \qquad (2)$$

Moreover, this theory predicts that the propagation properties of the line can be fully characterized by its four primary electrical per unit length (p.u.l) parameters namely : its resistance R, inductance L, capacitance C and conductance G. While the first two are derived from the conductor properties, the last two arise from the dielectric of the line. By denoting [Z] and [Y] respectively the impedance and admittance matrix of the transmission line, defined by $[Z]=R+j.\omega.L$ and $[Y]=G+j.\omega.C$, one obtains the equivalent circuit of an elementary portion of a multiconductor line as depicted in Fig. 4.

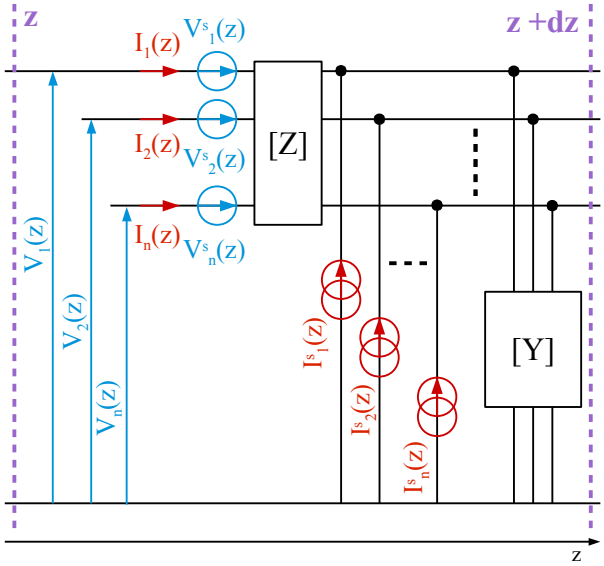

Fig. 4: Diagram of an elementary part of multiconductor transmission line

In the above outline, V^s and I^s stand respectively for voltage and current source terms that described electric and magnetic coupling between the line and its EM environment. Precise evaluation of those equivalent sources are of primary interest in EMC study. In the frame of MTLN theory, their estimation can be made through the knowledge of the tangential electrical field along the path of the line.

From the previous considerations, the propagation equation can be obtained from a

generalized expression of the well known telegraphers equation :

$$\begin{aligned}\frac{\partial[V(z)]}{\partial z}&=-[Z].[I(z)]+[V^s(z)]\\ \frac{\partial[I(z)]}{\partial z}&=-[Y].[V(z)]+[I^s(z)]\end{aligned} \quad (3)$$

In our case, it is useful to rewrite unknowns as the sum of two waves traveling in opposite directions, which gives for voltage part of equation (3) :

$$\begin{aligned}[V(z)]_+&=[V(z)]+Z_c(z).[I(z)]\\ [V(z)]_-&=[V(z)]-Z_c(z).[I(z)]\end{aligned} \quad (4)$$

where $[Z_c]$ and $[\gamma]$ are respectively the characteristic impedance and the propagating coefficient matrices of the line and are defined by :

$$\begin{aligned}[Z_c]&=[\gamma].[Y]^{-1}=[\gamma]^{-1}.[Z]\\ [\gamma]&=\sqrt{[Z].[Y]}\end{aligned} \quad (5)$$

This finally yields to expressions that we will further use :

$$\begin{aligned}\frac{\partial[V(z)]_+}{\partial z}+[\gamma].[V(z)]_+&=[V^s(z)]_+\\ \frac{\partial[V(z)]_-}{\partial z}-[\gamma].[V(z)]_-&=[V^s(z)]_-\end{aligned} \quad (6)$$

These equations are valid for each tube of the topological tree but they assume a prior determination of the V^s and I^s distributed sources and the knowledge of the RLCG primary electrical parameters. The next section discussed the method for evaluating these parameters.

3.2) Computation of the RLCG matrices

Determination of the electrical primary parameters is done using the electrostatic code *LAPLACE*, which is an integral part of the software suite *CRIPTE*™. This dedicated tool solves, by means of Method of Moments (MoM), the electrostatic equivalent problem (2) for an arbitrary cross-section. Indeed, it is proved that the capacitance matrix [C] can be directly deduced from the expression of the scalar potential (2) **[5]**.

As a first step, capacity matrix $[C]_0$ of the multiconductor line is computed in the absence of dielectric material. The inductance matrix is thus obtained from $[C]_0$ thanks to the following relation :

$$[L]=\frac{1}{c^2}.[C]_0^{-1} \quad (7)$$

In the presence of dielectrics around conductors, another computation is necessary to find the final capacitance matrix [C].

The conductance matrix [G] can also be obtained from the capacitance one by taking into account the complex part to the electrical permittivity.

Finally, the resistance matrix is the simplest to define since its value, corresponding to the linear resistivity of the wire, is an intrinsic property of conductors and can be directly measured. Nevertheless, we may take into consideration the frequency and thermal dependence due respectively to skin/proximity effects and Joule's heating. In this case, DC resistance value has to be rectified with an adapted coefficient depending on the material used and the layout configuration.

3.3) BLT equation

The key equation to find currents or voltage at any point of the network is the Baum-Liu-Tesche (BLT) equation. Its expression is established from the topology description of the electrical grid by combining propagation equation of waves over the network, as introduced in (4), and a generalized scattering equation which described waves distribution on junctions.

Unknown waves in the frame of BLT equation are direct ones, defined by :

$$(W(z))=(V(z))_+=(V(z))+Z_c(z).(I(z)) \quad (8)$$

By applying the change of variable $z'=z-L$ for retrograde waves, it appears that each end of the line is the starting point of a direct wave. Thus, we defined for each tube two direct waves

with opposite traveling directions as depicted in Fig. 5.

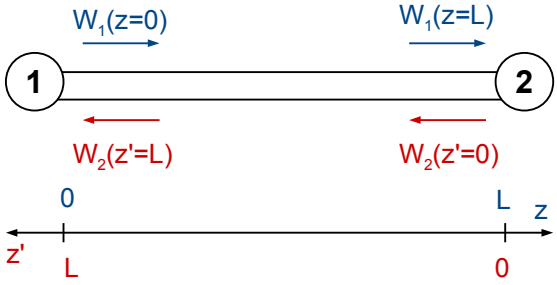

Fig. 5: Wave propagation over tube

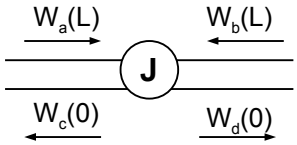

Fig. 6: I/O waves at an arbitrary junction stage

It then follows that the transmission of a wave along a tube takes the following formulation :

$$[W(L)]=[\Gamma].[W(0)]+[W^s]$$

with :

$$[W(0)] = \begin{bmatrix}[W_1(z=0)]\\ [W_2(z'=0)]\end{bmatrix}$$

$$[\Gamma] = \begin{bmatrix} e^{-[\gamma].L} & [0] \\ [0] & e^{-[\gamma].L}\end{bmatrix} \qquad (9)$$

$$[W^s] = \begin{bmatrix} \int_0^L e^{-[\gamma].(L-z)}.[V^s(z)]_+.dz \\ \int_0^L e^{-[\gamma].(L-z')}.[V^s(z')]_+.dz' \end{bmatrix}$$

Junctions, that can represent both load impedance or simply dispatching node of EM waves, ensure electrical continuity over the network. Consequently, one has to define the scattering [S] matrix associated with each of them. For an arbitrary junction we therefore get, as related to Fig. 6 :

$$\begin{cases} W_c(0)=[S_{ca}].[W_a(L)]+[S_{cb}].[W_b(L)] \\ W_d(0)=[S_{da}].[W_a(L)]+[S_{db}].[W_b(L)] \end{cases} \qquad (10)$$

Which we can rewrite in :

$$[W(0)]=[S].[W(L)]$$

$$\text{with : } [S]=\begin{bmatrix}[S_{ca}] & [S_{cb}] \\ [S_{da}] & [S_{db}]\end{bmatrix} \qquad (11)$$

Finally, the propagation equation coupled to the generalized scattering equation leads to the BLT equation for the whole network :

$$([\boldsymbol{Id}]-[S].[\Gamma]).[W(0)]=[S].[W^s] \qquad (12)$$

where $[\boldsymbol{Id}]$ is the identity matrix

Once the algebraic system is solved, i.e the starting waves [W(0)] are determined for all junctions, one can retrieves voltage and currents at every point of the network by means of equations (4) and (9).

4) Thermal modeling

The purpose of the thermal simulation is to predict, from a topological representation of the EWIS, the total amount of heat produced by groups of cables. Although norms and abacus exist, these ones are often inaccurate in a wide range of practical applications and thus tend to overestimate the temperature of such bundles **[6]**.

4.1) Heat Equation

To ensure precise calculations, our approach has been to directly solve the Heat Equation, whose general expression in steady state case is given by :

$$\nabla.(\lambda \nabla \mathbf{T})+q_{gen}=0 \qquad (13)$$

where λ is the thermal conductivity of the material [W/(m.K)]. If we assume constant Joule heating, then the volume heat source (expressed in W/m^3) can be computed by :

$$q_{gen}=\frac{\rho.I_{eff}^2}{\pi^2.r^4} \qquad (14)$$

with : I_{eff}, the efficient current flowing through a wire (A) of radius r (m) and linear electrical resistivity ρ ($\Omega.m$).

Basically, we took the following expression for boundary condition :

$$\lambda\frac{\partial T}{\partial \boldsymbol{n}}=h[T_\infty-T]+\epsilon\sigma[T_\infty^4-T^4] \qquad (15)$$

where h represents the convective transfer coefficient, T_∞ the ambient temperature, ε the thermal emissivity of the surface and σ the Stefan-Boltzmann constant.

Convective and radiative contributions are often put in an overall transfer coefficient which simplifies (15) :

$$\lambda \frac{\partial T}{\partial \boldsymbol{n}} = h(T)[T_\infty - T] \qquad (16)$$
$$\text{with : } h(T) = h_{conv}(T) + h_{rad}(T)$$

4.2) Heat transfer coefficient

The main challenge here arises in the precise determination of the coefficient of convective heat transfer h_{conv} , which strongly depends on the thermal environment (ambient temperature and pressure), on the nature of the flow (natural or forced convection) around the harness as well as the installation conditions of the wiring. Indeed, its value may fluctuate rapidly due to change of one of these parameters and this issue constitutes a very complex non-linear problem of fluid mechanics.

Because there is no general expression for this coefficient, we must estimate it for each case of interest by means of empirical correlations or experimental measurements.

5) Coupling strategy

To optimize total mass of wiring considering both thermal and EMC constraints, two ways of proceeding can be considered. The first one is to modify the diameter of wires composing the bundle while the second one consists in a cross-section reshaping. Such optimization principles are described in **[6]**.

As illustrated on Fig. 11, the electrostatic and temperature computations both involve a Poisson's equation, with a different set of coefficients for each physics.

Indeed, temperature and electrostatic field are derived from the same potential notion **[7]**. Hence, when applying to a cable bundle, a single resolution of the Laplacian must give the p.u.l properties of the transmission line and its temperature distribution *at the same time*. Couplings between thermal and electromagnetic phenomena are therefore totally defined by the characteristics of the electrical currents (intensity, frequency), the thermal properties of materials and the estimation of the heat transfer coefficient to the surrounding environment.

In the aim of providing a unique computational tool for both thermal and EMC issues, Poisson's equation has first to be expressed in its integral formulation as detailed in Fig. 8.

Classical formulation of Poisson's equation

$$\nabla . (\kappa \nabla \boldsymbol{F}) = S$$

	Electrostatic equivalent problem	Steady state heat equation
κ	ε *(electrical permittivity)*	λ *(thermal conductivity)*
F	Φ *(scalar potential)*	T *(temperature)*
S	0	$-q_{gen}$ *(heat source)*

Fig. 7: Equivalence between electrostatic and steady state thermal problems

Integral equations are aimed to be solved only at frontiers of the geometry. Hence, the final potentials are obtained anywhere on the cross-section by combining results of each sub-domain boundaries. Since no analytical solution exists to these equations except for very particular case, one has to use a numerical method to solve them. In our case, this is done through the Method of Moments where solution F is interpolated by a set of known basis functions like expressed below :

$$F = \sum_{i=0}^{+\infty} a_i . f_i \qquad (17)$$

These functions are then weighted by other ones called "test" functions :

$$< u_p , F > = \int_\Gamma u_p . \sum_{i=0}^{+\infty} a_i . f_i \, dS \qquad (18)$$

Finally, the contour Γ, which represents boundary of an arbitrary domain, is sampled in finite number of segments or radius sections according to which shape is the most appropriate for it. This yields to a general matrix equation where the unknown vector contains the a_i coefficients weighting F.

Although mathematically these equations are part of the same resolution frame, from a physics point of view the distinction between the EMC and thermal calculations is made when

applying their different boundary condition : Dirichlet kind for electrostatic problem (imposed potential of the ground returning plane) and modified Robin kind for thermal issue as stated in (15). However, except for the matrix blocks directly attached to boundary conditions, the matrix that gathers interactions between Green's functions G (the fundamental solution of the Laplacian) and the basis functions can be used by both calculations because it only depends on the shape of the cross-section.

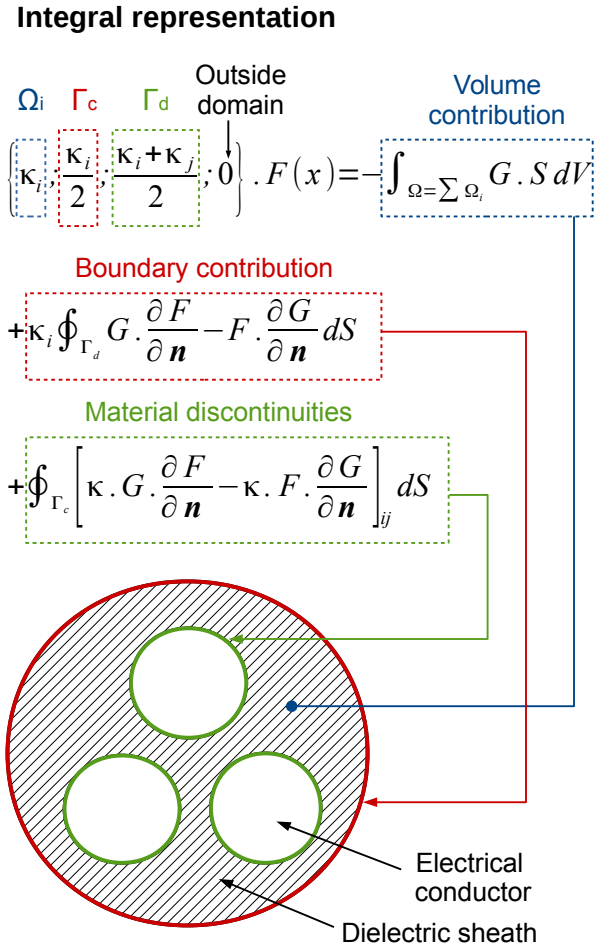

Fig. 8: Integral formulation of Poisson's equation. Application to a simplified three-phase cable

Thus, this allows the simultaneous computation of the electrostatic potential and of the temperature field. It also enables fast recalculations when the layout configuration remains unchanged, because time-consuming operations can be avoided as they are just made once (in particular, the interaction matrix stays the same).

This property is useful when thermo-physical properties of materials must be taken into consideration. The whole coupling strategy is summarized in Fig. 9.

Currently, a thermal solver which solves the heat equation by means of Method of Moments has been developed apart from *CRIPTE™* software. However, the loop consisting of the injection current update is already effective and allows us, as we will see in the next section, to conduct coupled EMC and thermal simulations.

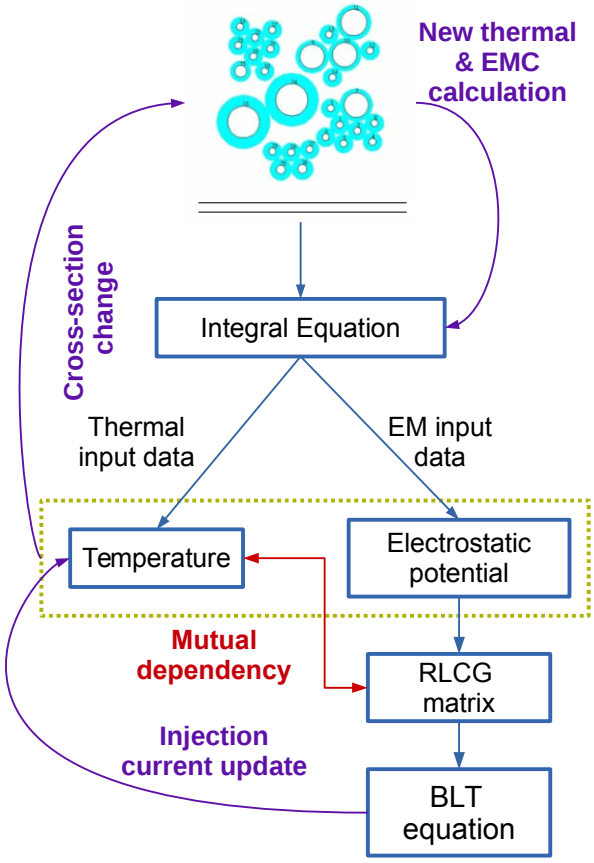

Fig. 9: General coupling strategy and optimization loop

6) Application to complex bundle

An application case has been defined as a bundle of 11 cables inserted into an insulator sheath and placed in free air.

In a first simulation only three cables have been fed with TTL signals of 200 kHz frequency and cycle ratio 0.5. Respective RMS intensity of 11 A, 8 A and 33 A were carried by wires 2, 7 and 9 (Fig. 10). Other cables have been short-circuited in order to emphasize crosstalk currents.

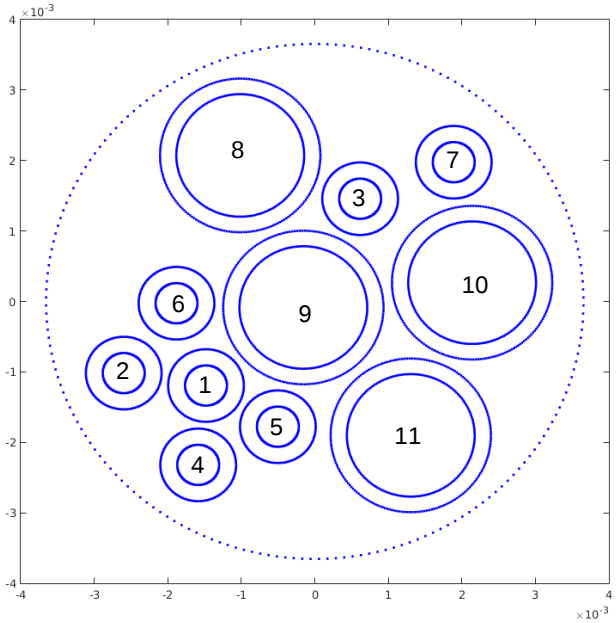

Fig. 10: Bundle cross-section and cable numeration

As a first step, topological and geometry description is made using *CRIPTE™* software. On the unique defined tube, powered cables were connected by a 1 Ω impedance to a ground reference plane located 5 centimeters below. The bundle length was set to 1 meter.

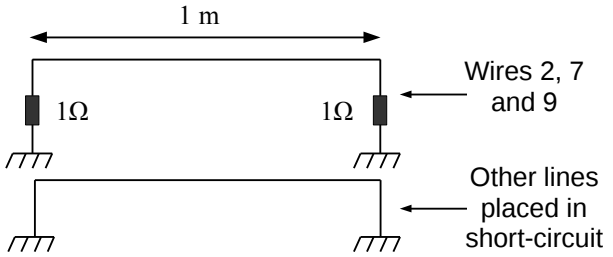

Thermal conductivity [W/(m.K)] : 401 (copper), 0.33 (dielectric), 0.1 (sheath)
Ambient Temperature (°C) : 25
Electrical conductivity (S/m) : 59.6e6
Boundary condition : free space convection and radiation → constant value *h=10 W/(m².K)*

Fig. 11: Main characteristics of the studied line

Cross-section, whose schema is given by Fig. 10, has been generated randomly from geometrical and physical description established by *CRIPTE™* and its integrated tool *ALEACAB*.

In the following simulations, thermophysical properties of materials are neglected. The variation of the electrical resistivity as a function of frequency is also disregarded because the skin effect depth is close to the dimension of wires. Thermal boundary condition is natural convection in free air with a constant heat coefficient transfer.

As shown in Fig. 12, a first thermal calculation is made solely from the the injection voltage. At this stage, no *CRIPTE™* computation is done and the effect of the crosstalk currents does not appear in the temperature result.

Wire	Initial RMS currents injection (A)	RMS currents computed with CRIPTE (A)
1	0	4.65
2	11	10.09
3	0	3.79
4	0	1.46
5	0	2.62
6	0	5.04
7	8	7.36
8	0	5.84
9	33	32.06
10	0	6.61
11	0	3.93
Total heat generated (W)	19.38	22.78

Table 1: Currents and total heat generated for the first test case

In a second stage, a *CRIPTE™* calculation enables us to evaluate the currents on each wire of the bundle. These currents are then averaged and injected in the thermal solver as volume heat source power by means of equation (14). Final values for currents and heat generated are given in Table 1. Results show an increase of the temperature up to 16 °C, and we can note that this overheating is especially located on wires 1 and 6. Indeed, these ones were placed in close proximity to the two voltage injections (wire 2 and 9).

However, due to electromagnetic laws of induction and energy conservation, the efficient currents flowing on those powered wires have been filtered and reduced in regards to the initial injection, and the part of lost currents ended up exactly on the wires placed in short-circuit.

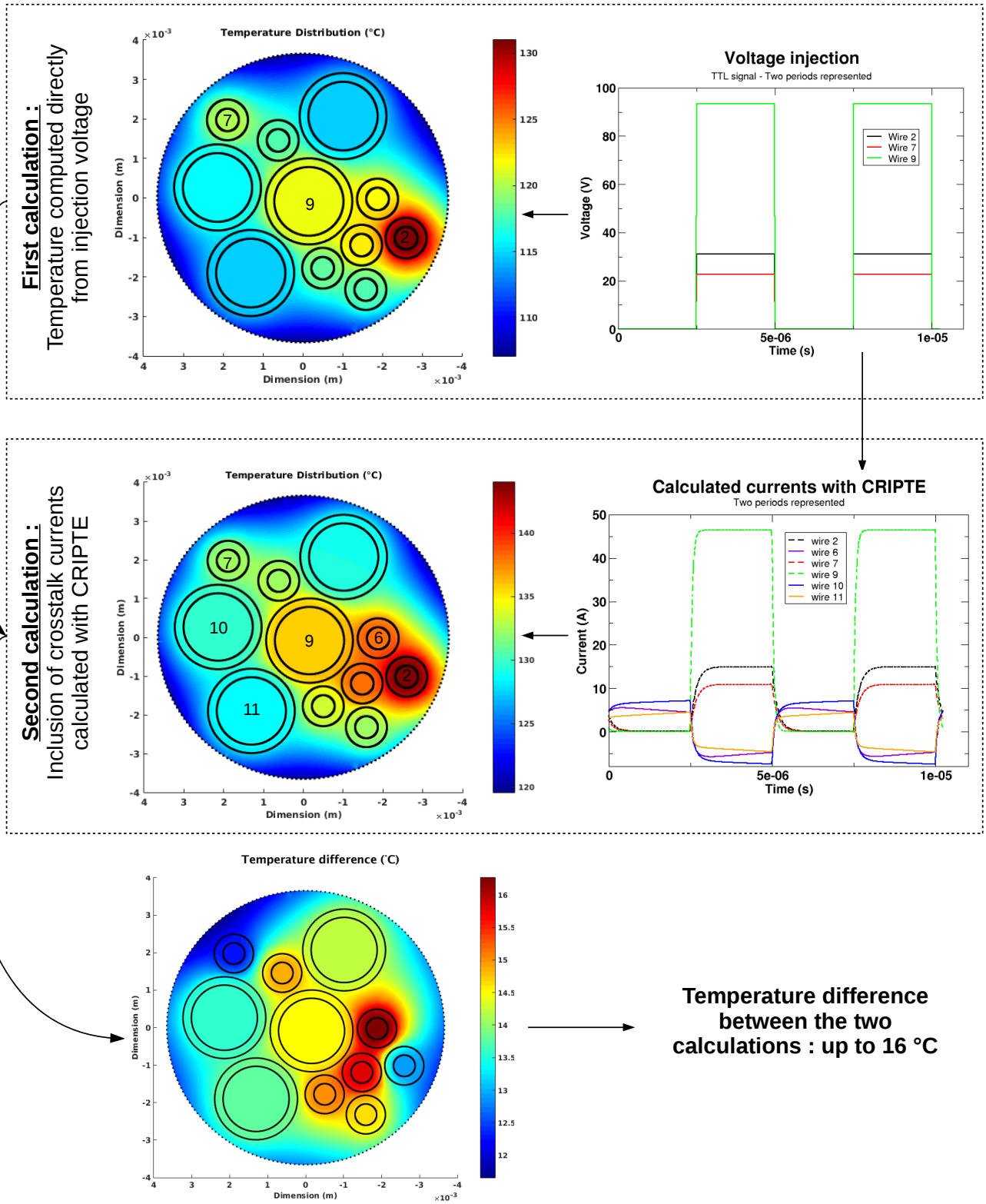

Fig. 12: First test case results

Although injection cables produce less heat, this reduction is largely offset by the heat produced by the induced currents flowing on those short-circuited cables.

In order to analyze the crosstalk currents contribution on the total heat generation, another simulation has been conducted. In this second test case, the same simulation plan as previously stated has been followed, but a difference lied in the number of fed wires : while number 7 and 9 were turned off (but still matched to the 1 Ω impedance), wire 2 still carried a 11 A RMS current. In this case, the temperature difference between simulations with fixed and calculated currents by *CRIPTE™* was smaller than 2 degrees at least as shown in Fig. 13, contrary to what was observed for the first test case.

Wire	Initial RMS currents injection (A)	RMS currents computed with CRIPTE (A)
1	0	2.13
2	11	10.13
3	0	0.04
4	0	1.28
5	0	0.18
6	0	2.17
7	0	0.01
8	0	0.63
9	0	0.2
10	0	0.1
11	0	0.19
Total heat generated (W)	7.76	7.46

Table 2: Currents and total heat generated for the second test case

Indeed, as shown in Table 2, more heat had been generated when crosstalk currents were disregarded. By looking carefully at relation (14), one can see that the amount of heat created by Joule's effect depends not only on the square of the effective current but also on the inverse of the fourth power of the radius. This emphasizes that a better current distribution between small and large wires leads to less heat generated even though these induced currents are far from irrelevant.

7) Conclusion and perspectives

The need for coupled EMC and thermal modeling has been demonstrated as both aspects significantly impact on the total heating of cable bundles.

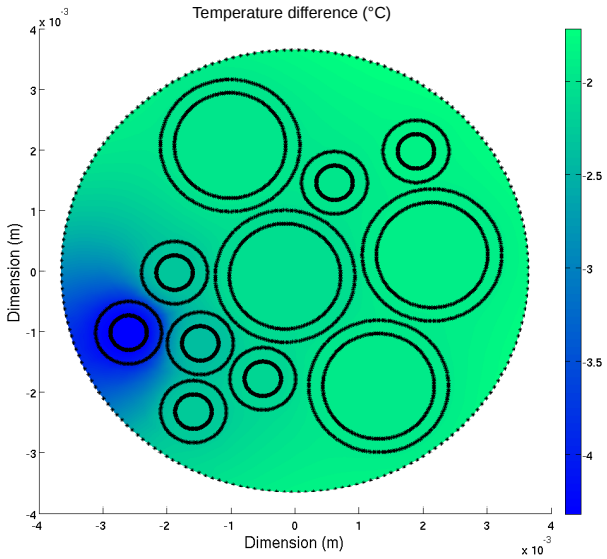

Fig. 13: Temperature difference for the second test case (scale is negative)

Future works will include the complete integration of the thermal tool into *CRIPTE™* software and the development of an optimization procedure in order to reduce, from EMC and thermal criteria, the mass of a given EWIS.

In order to refine our thermal model, especially on convective coefficient issues, an experimental workbench should be built shortly. Its objectives will be twofold. On the one hand it will validate numerical results given by the tool specially developed. On the other hand it will provide a database of heat transfer coefficient for some EMC case of interest : bundle in free air, above a ground plane or placed into a raceway. The setup will be composed of a climate chamber with temperature controlled walls and adaptable height. The velocity field of the airflow around the bundle will be measured by means of Particle Image Velocimetry (PIV) technique, which allows to retrieve an estimation of the convective heat transfer coefficient *h*. Concerning temperature measurement, we will widely inspire of **[8]** and should use surface thermocouple probes placed on interesting

points of the wiring. The drawing of the future setup is given by Fig. 14.

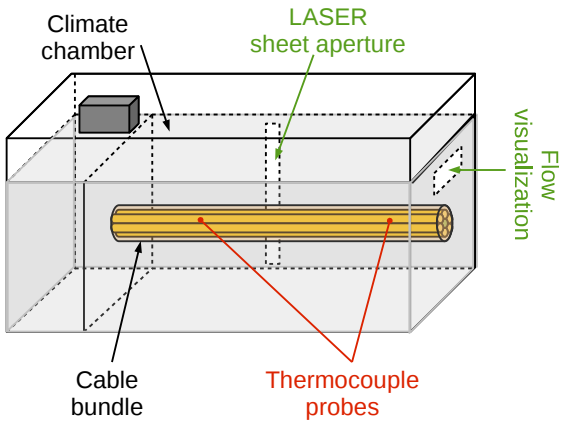

Fig. 14: Drawing of the experimental workbench

References

[1] X. Roboam and al, *"More Electricitiy in the air – Toward Optimized Electrical Networks Embedded in More Electrical Aircraft"*, IEEE Industrial Electronics Magazine, Dec. 2012.

[2] P. Millan and al, *« Evolution en CEM et en thermique dans l'avion encore plus électrique »*, French conference on Towards even more electrical aircraft, REE N°6/7 (June/July) 2009.

[3] C.E. Baum, T.K. Liù, and T.E. Tesche, *"On the Analysis of General Multiconductor Transmission-Line Networks"*. Interaction Notes, Note 350, November, 1978.

[4] M. Ridel, J.P. Parmantier, C. Girard and C. Giraudon, *"Methodology for modelling EM coupling on EWIS"*, MEA Bordeaux 2012.

[5] L. Paletta, *« Démarche topologique pour l'étude des couplages électromagnétiques sur des systemes de cablages industriels de grandes dimensions »,* Université Paris XI-Orsay, phD dissertation (in French) , 1998.

[6] F. Loos, *"Joule Heating in Connecting Structures of Automotive Electric Devices"*, Universität der Bundeswehr München, phD Dissertation, 2014.

[7] R.P. Feynman, *"The Feynman Lectures on Physics. Vol. II – Mainly Electromagnetism and Matter Basic"*, Basic Books, 2014.

[8] A. Ilgevicius, *"Analytical and Numerical Analysis and simulation of heat transfer in electrical conductors and fuses"*, Universität der Bundeswehr München, phD Dissertation, 2004.

Acronyms

CAC : Core Avionic Cabinet

EM : Electromagnetic

EMC : Electromagnetic Compatiblity

EMI : ElectroMagnetic Interference

LB : Load Box

RMS : Root Mean Square

TTL : Transistor-Transistor Logic

Copyright Statement